Possible power of down-regulated offshore wind power plants

Göçmen, Tuhfe; Giebel, Gregor; Poulsen, Niels Kjølstad; Sørensen, Poul Ejnar

Published in:
Wind Energy

Link to article, DOI:
10.1002/we.2279

Publication date:
2019

Document Version
Publisher's PDF, also known as Version of record

Received: 18 August 2017 | Revised: 24 August 2018 | Accepted: 31 August 2018
DOI: 10.1002/we.2279

WILEY

RESEARCH ARTICLE

Possible power of down-regulated offshore wind power plants: The PossPOW algorithm

Tuhfe Göçmen[1] | Gregor Giebel[1] | Niels Kjølstad Poulsen[2] | Poul Ejnar Sørensen[1]

[1]DTU Wind Energy, Technical University of Denmark, Risø Campus, Roskilde, Denmark
[2]DTU Compute, Department of Applied Mathematics and Computer Science, Technical University of Denmark, Kongens Lyngby, Denmark

Correspondence
Tuhfe Göçmen, DTU Wind Energy, Technical University of Denmark, Risø Campus, Frederiksborgvej 399, 4000 Roskilde, Denmark.
Email: tuhf@dtu.dk

Funding information
Energinet.dk, Grant/Award Number: 2012-1-10763 and 2016-1-12396

Abstract

This paper proposes a method for real-time estimation of the possible power of an offshore wind power plant when it is down-regulated. The main purpose of the method is to provide an industrially applicable estimate of the possible (or reserve) power. The method also yields a real-time power curve, which can be used for operation monitoring and wind farm control. Currently, there is no verified approach regarding estimation of possible power at wind farm scale.

The key challenge in possible power estimation at wind farm level is to correct the reduction in wake losses, which occurs due to the down-regulation. Therefore, firstly, the 1-second wind speeds at the upstream turbines are estimated, since they are not affected by the reduced wake. Then they are introduced into the wake model, adjusted for the same time resolution, to correct the wake losses. To mitigate the uncertainties due to dynamic changes within the large offshore wind farms, the algorithm is updated at every turbine downstream, considering the local axial and lateral turbulence effects.

The PossPOW algorithm uses only 1-Hz turbine data as inputs and provides possible power output. The algorithm is trained and validated in Thanet and Horns Rev-I offshore wind farms under nominal operation, where the turbines are following the optimum power curve. The results indicate that the PossPOW algorithm performs well; in the Horns Rev-I wind farm, the strict power system requirements are met more than 70% of the time over the 24-hour data set on which the algorithm was evaluated.

KEYWORDS

available power, possible power, real-time power curve, real-time wake modelling

1 | INTRODUCTION

The share of offshore wind power is continuously increasing, especially in the Northern European grids. Together with other renewables, the accelerated implementation of offshore wind power implies many technical challenges. Particularly that the electricity system needs to adjust to the decentralized and highly variable production. To assure safety in the operation of the power system, offshore wind farms are designed as wind power plants (WPPs) required to contribute to the stability of the grid by offering grid services (also called ancillary services). As part of those services, offshore WPPs provide operating reserve capacity to the electricity network, which is activated by down-regulating the wind farm from its maximum possible power.[1-3] The estimation of the available power, or eventually the reserve capacity, is essential as the balancing responsible parties are compensated for this service in terms of the level of reserves, regulated by the national grid code. The reserve power can also be traded in the balancing market, depending on the regional market schemes. What is seen from the existing European regulations[4] is that adequate and standardized regulations or technical requirements to help in understanding the possible power or the amount of reserves for their system reliability is lacking. This research is critical not only for the power system stability but also for the business case of wind energy.

Individual wind turbines already have a supervisory control and data acquisition (SCADA) system signal called possible[5] or available[6] power, depending on the turbine manufacturer. However, the sum of those individual signals is a clear overestimation of the available power of a down-regulated wind farm; simply because the wind speed is higher at the downstream turbine location(s) due to the decrease in wake losses under curtailment. In fact, taking advantage of the reduction in the wake losses behind down-regulated turbine(s) to optimize the power production while minimizing turbine loads is one of the prominent fields in wind farm control.[7-10] Distinctly from the wake control community, where the main focus is to model the "down-regulated" wake, here, we aim to correct the reduced wake effects within a curtailed wind farm to simulate the nominal power output. Note that, especially for large offshore wind farms, the turbine data, also referred to as SCADA data, are the most available and representative of the local flow and operational characteristics. Here in this study, the possible power estimation is based purely on the high-frequency (1 Hz) turbine data as opposed to the high fidelity wind farm simulations. Consequently, we introduce a pragmatic real-time wake modelling/calibration approach and provide an industrially applicable method to estimate the available power of a wind farm in the frame of the PossPOW project.[11] When applied during nominal operation, the algorithm clearly provides a real-time (1 Hz) wind farm power curve that can then be fed into the control system.

In the PossPOW algorithm, the rotor effective wind speed is calculated at every second at the curtailed upstream turbines that are not affected by the down-regulated wake. As illustrated in Figure 1, the wind speed estimation approach takes (active or produced) power, rotational speed, and pitch angle signals as inputs from the SCADA system, in addition to the temperature and pressure used to correct the local air density. It was developed and validated during both down-regulation and normal operation using 1 Hz met mast and SCADA data from the Horns Rev-I, Lillgrund and Thanet offshore wind farms, together with NREL 5MW simulations.[12,13] The results indicate that the output of the rotor effective wind speed estimation module, U_{eff}, performs considerably better than the nacelle anemometer with significant reduction in uncertainty and less than 5% mean absolute error compared with the met mast measurements.

In order to replace the down-regulated wake with the nominal case, the upstream wind should be read by the wake model to estimate the velocity deficit that would occur during normal operation. However, most of the robust wake models are tuned and verified for 10-minute averaged data and used to acquire long term, statistical information.[14-16] Therefore, the analytical model proposed by Larsen[17,18] is recalibrated

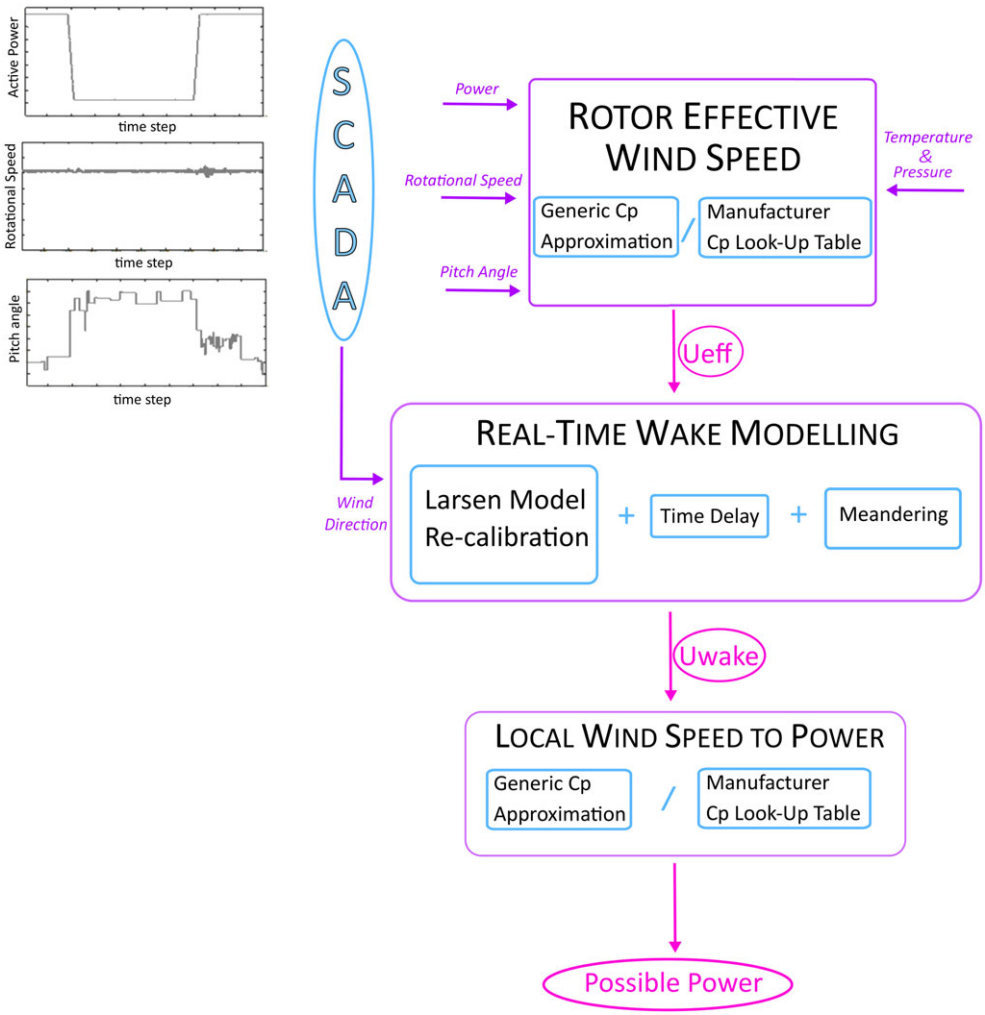

FIGURE 1 PossPOW (representative) inputs and work flow. SCADA, supervisory control and data acquisition [Colour figure can be viewed at wileyonlinelibrary.com]

for a single wake case in Thanet offshore wind farm, validated in Horns Rev-I and then implemented in both of the wind farms considering the local turbulence, time delay, and meandering. The wake velocity, U_{wake}, is calculated at each turbine in the wind farms and, depending on the availability of the turbines' power coefficient information, converted to power. It should be noted that, due to the modular structure of the PossPOW algorithm, both incoming wind speed assessment and the real-time wake modelling is adjustable. For example, the rotor effective wind speed estimation of the upstream turbines can easily be replaced by met mast or lidar measurements where available. Similarly, another low-cost wake model can be implemented instead of the Larsen model (eg, Bastankhah and Porté-Agel[19] or purely data-driven algorithms such as Japar et al[20]). As a side note, the selection of the Larsen model is fundamentally based on its explicit handling of turbulence intensity and history of successful offshore implementation. The wake model selection will be elaborated upon later.

Firstly, the data extracted from SCADA systems for the case studies of Thanet and Horns Rev-I offshore wind farms are detailed in section 2. The first module of the algorithm, the estimation of the rotor effective wind speed, is described based on previous work in section 3. The recalibration of the Larsen model for the single wake case, together with the time delay estimation and meandering correction are presented in section 4.

Since the wind farm scale possible power is not measurable by definition, the validation of the algorithm is nontrivial. Here in this study, the PossPOW output is tested on nominal operation data sets where the wind farm production is set to match the possible power. The implementation of the real-time wake modelling to the wind farm scale and the evaluation of the algorithm is presented in section 5. The resulting possible power estimations for both Thanet and Horns Rev-I are analysed with respect to the strict requirements from Danish Transmission System Operator (TSO) Energinet.dk.[1] The regulations state the possible power estimation to be submitted as 5-minute time series and transferred to Energinet.dk once a day, and the error of the provided calculations are to be within ±5% span of the actual production. In this respect, the evaluation of the PossPOW algorithm is based upon the percentage error distribution in Thanet and Horns Rev-I wind farms during nominal operation. The validation of the algorithm under down-regulation can only be performed via full-scale field tests, which is left as a future work for this study.

2 | SITES AND DATA

As indicated earlier, the PossPOW algorithm is designed to work with 1-Hz SCADA signals from individual turbines within the wind farms. The details of the extracted signals and investigated offshore WPPs are presented in this section.

2.1 | Thanet offshore wind farm

The Thanet offshore wind farm is located in the eastern United Kingdom, approximately 15 km away from the nearest shore. The wind farm consists of 100 Vestas V90-3MW offshore turbines. The turbine diameters are 90 m, and the hub is located at 70 m height. The distance between the turbines is approximately 480 m corresponding to 5.3 diameters, or 5.3*D*, for the perpendicular wind direction, 317°. In Figure 2, the layout of the wind farm is presented, together with the Vestas V90-3MW standard power and thrust curve.

The 1-Hz data set used in the analysis is extracted for north-westerly winds, ie, 317° ± 20°. The provided 1-Hz SCADA signals are active power, *P*; rotational speed, ω; pitch angle, θ; nacelle wind speed (measured by nacelle anemometers), *NWS*; average temperature; wind direction (yaw angles); and possible power (turbine level). After filtering for wind direction, the resulting data for the recalibration consists of 24 960 seconds that corresponds to approximately 7 hours.

2.2 | Horns Rev-I offshore wind farm

The Horns Rev-I wind farm is located in western Denmark, approximately 14 km away from the coast and consists of 80 Vestas V80-2MW turbines. The hub height of the installed turbines is 70 m while the rotor diameter is 80 m. Horns Rev-I is one of the most commonly studied wind farms with a regular, slightly inclined layout as shown in Figure 3.

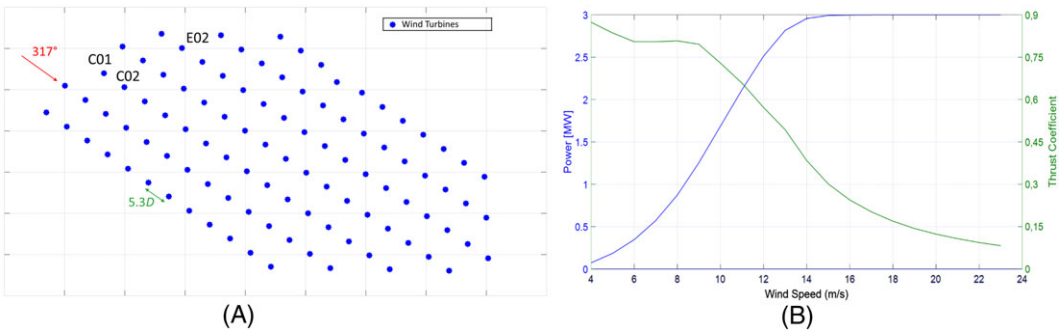

FIGURE 2 A, Layout of the Thanet offshore wind farm and B, Vestas V90-3MW offshore turbine power, *P*, and thrust coefficient, c_T, curve[21]
[Colour figure can be viewed at wileyonlinelibrary.com]

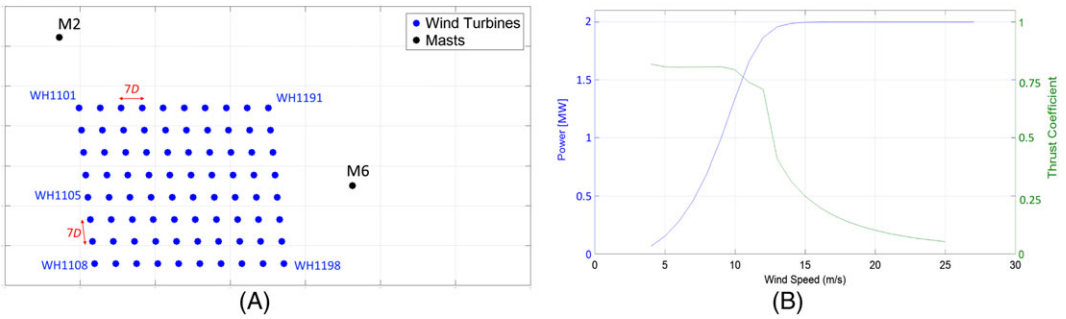

FIGURE 3 A, Layout of the Horns Rev-I offshore wind farm and B, Vestas V80-2MW offshore turbine power, P, and thrust coefficient, c_T, curve[22] [Colour figure can be viewed at wileyonlinelibrary.com]

TABLE 1 The coefficients used in the effective wind speed estimation

$\mathbb{C}_1$	$\mathbb{C}_2$	$\mathbb{C}_3$	$\mathbb{C}_4$	$\mathbb{C}_5$	$\mathbb{C}_6$	$\mathbb{C}_7$	$\mathbb{C}_8$	$\mathbb{C}_9$
0.47	101	0.4	0.01	1.95	5	16.5	0.089	0.02

The single wake validation data set in Horns Rev-I consists of easterly winds, ie $90^\circ \pm 20^\circ$ covering a period of 77 950 seconds, approximately 21.5 hours. The same 1-Hz SCADA signals as in the Thanet case are extracted from the turbines. For the wind farm scale calculations, a consecutive 24-hour data set is presented in terms of 5-minute averaged values to provide a daily visualization. Note that the upstream wind direction signals both in Horns Rev-I and Thanet are corrected from the bias using the maximum wake depth along the perpendicular incoming flows.[23]

3 | ROTOR EFFECTIVE WIND SPEED

As illustrated in Figure 1, the first module in the PossPOW algorithm is to estimate the local wind speed at the upstream turbines. The incoming wind speed is to be input into the wake model to assess the nominal wake and estimate the possible power. Under normal operation and below the rated power region, the common practice is to use the power curve approach when a meteorological mast is not available (eg, Hansen et al[24] and Nygaard[25]). However, since the algorithm is designed for down-regulation conditions, the power curve wind speed approach is not applicable. Additionally, the anemometers mounted on the nacelle are exposed to highly distorted flow.[26] Particularly for real-time calculations, using nacelle wind speed measured during relatively shorter periods may induce higher uncertainties.[27] Therefore, the rotor effective wind speed method, which is validated on Horns Rev-I, Thanet, and Lillgrund offshore wind farms,[12,13] is applied at the turbine locations and used for recalibration and validation processes of the PossPOW algorithm. As well as the basic rotor geometry, the wind speed estimation procedure (Equation 1) takes active power, pitch angle, and rotational speed signals of the turbine to iteratively estimate the effective wind speed.

$$\begin{aligned} P &= \frac{1}{2}\rho C_P(\lambda,\theta)\pi R^2 U_{eff}^3, \quad \text{with} \\ \text{Approximated } C_P(\lambda,\theta) &= \mathbb{C}_1\left(\frac{\mathbb{C}_2}{\lambda_i} - \mathbb{C}_3\theta - \mathbb{C}_4\theta^{\mathbb{C}_5} - \mathbb{C}_6\right) exp\left(\frac{-\mathbb{C}_7}{\lambda_i}\right), \quad \text{where} \\ \lambda_i &= \left[\left(\frac{1}{\lambda + \mathbb{C}_8\theta}\right) - \left(\frac{\mathbb{C}_9}{\theta^3+1}\right)\right]^{-1}, \end{aligned} \tag{1}$$

where ρ is the air density, λ is the tip speed ratio, and U_{eff} is the incoming effective wind speed. The power coefficient, $C_P(\lambda,\theta)$, required to solve Equation 1 for wind speed can be defined by the original look-up table provided by the manufacturer when available. For this study, the turbine data from Vestas V80 and V90 were not accessible. Therefore, the $C_P(\lambda,\theta)$ is approximated based on Equation 1 and the constants fitted in Göçmen et al[12] are listed in Table 1. In Göçmen and Giebel,[13] a very good agreement is observed between the approximated and the original $C_P(\lambda,\theta)$, where the mean error is less than 3%. The methodology is applied to both the upstream and the downstream turbine(s).

After the wind speed is estimated at the upstream turbine locations, a real-time integrated wake model can be applied to remove the reduced wake effects and simulate the nominal operation conditions within the wind farm.

4 | REAL-TIME WAKE MODELLING

Accurate prediction of wake effects has been a key focus area in wind energy research from the individual turbine level,[28] to a group of turbines,[29] and wind farm level.[16,30] Most of the existing computationally affordable wake models are tuned and validated for 10-minute data to simulate steady-state, long-term behaviour. However, in order to comply with the grid requirements regarding wind farm possible power estimation, dynamic simulations that are capable of representing short-term performance are required. Such quasi-dynamic wake models would also enable

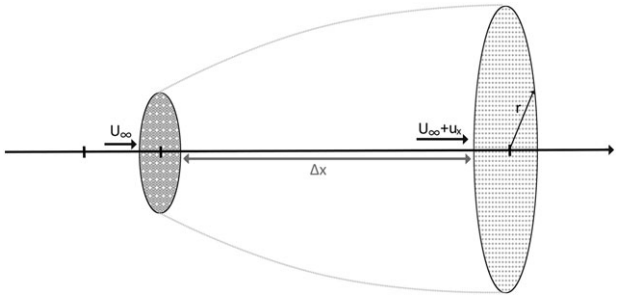

FIGURE 4 Control volume of the Larsen wake model (adapted from Larsen[17])

to monitor the wind farm operation on-line and develop active control strategies accordingly. Instead of introducing yet another wake model, here, we choose to recalibrate the Larsen wake model[17,18] as it is robust and fast, hence suitable for real-time (1 Hz) applications, and is shown to perform well also offshore.[16,31] Since the PossPOW algorithm is to perform short-term power estimations for the time intervals smaller than usual 10-minute bins, the computational speed is important, and high fidelity models are avoided.

The Larsen wake model has been implemented in many engineering applications due to its practicality and simplicity. In the model, the axisymmetric form of Reynolds Averaged Navier Stokes (RANS) equations with thin shear layer approximation is used; the control volume considered in the equations is illustrated in Figure 4. The turbulence closure was represented using Prandtl's mixing-length theory. After performing an order of magnitude analysis, Larsen has considered the solution in two parts; first and second order approximations where the latter was found to be negligible for most engineering applications. The final version of the axial velocity deficit equation is obtained as[17]

$$u_x(x,r) = -\frac{U_\infty}{9}(c_T A x^{-2})^{1/3}\left\{r^{3/2}(3c_1^2 c_T A x)^{-1/2} - (35/2\pi)^{3/10}(3c_1^2)^{-1/5}\right\}^2, \tag{2}$$

where u_x is the wake perturbation of the inflow in the axial direction, U_∞ is the free-stream point-wise inflow velocity, c_T is the thrust coefficient, $A = \pi R^2$ is the rotor swept area, R is the rotor radius, and r is the radial direction originated at the hub. Also note that the modelled radius of the wake, R_w, is proportional to the cube root of the distance, ie, $R_w \sim x^{1/3}$. The parameters to calibrate using 1-Hz field data are c_1, which is explicitly seen in Equation 2 and x_0, which is embedded in $x = x_0 + \Delta x$, where Δx is the axial distance between the turbines. The term x_0 represents the distance between the origin of the asymptotic wake and the position of the wake generating turbine. It is bounded to be positive in the frame of reference, $x_0 > 0$, as illustrated in Figure 4.

4.1 | Recalibration of the Larsen wake model

Because the calibration is to be performed using rotor effective wind speeds, the point-wise wake deficit u_x in Equation 2 needs to be averaged over the rotor. Gaussian 4-point integration is applied to estimate the wind speed distribution over the rotor using the same Gauss weights and the associated integral variables as in the original model.[18] The numerical integration of Equation 2 in this manner gives the effective wake deficit, u_{eff}, in terms of incoming effective wind speed U_{in}, the thrust coefficient c_T, the rotor radius R, and the axial distance between the turbines Δx, together with the calibration parameters c_1 and x_0

The recalibration of the Larsen model is performed for a single wake event in Thanet considering the turbines C01 and C02 for $317^\circ \pm 15^\circ$ incoming wind direction; see Figure 2. More than one turbine pairs were considered to capture a clear wake shape; however, C01 to C02 have the least number of "outliers" in terms of the upstream side winds due to the wind farm layout. Note that the wind direction bin of 15° for the investigated period ensures that the parameters are tuned for the wake events only. The radius of the Vestas V90-3MW offshore turbines are $R = 45$ m, and the distance between the turbines for considered wind direction is taken to be $\Delta x = 5.3D$ in Equation 2.

4.1.1 | Time delay concept

Before using the data set to determine the parameters c_1 and x_0 for the single wake, the time it takes for a particle to move from the most upstream turbine to the turbine in question, t_d, is taken into account by applying a correction to the calibration data set.

Machefaux et al[32] studied the advection time in detail, in which the cross-correlation between the measured near wake velocity profiles are investigated. The time lag between the downstream lidar measured patterns is quantified as the specific time shift where the profiles are most correlated. On the other hand, the lack of measurement campaigns in considered wind farms and the operational framework of this study limit the analysis to be performed only at the turbine locations, using the turbine data. Therefore, the proposed methodology is simply $t_{down} = t_{up} + t_d$ where t_{down} and t_{up} are the time steps when the same particles in the flow hits the downstream and the upstream locations, respectively. The order of magnitude analysis between the axial distance and the wake deficit in Equation 2 yields $u_x(x) \sim x^{-2/3}$, where $u_x(x)$ is the wake advection velocity to estimate the time delay.

Note that the distance between the turbine in question and the most upstream turbine is equal to Δx for the single wake recalibration case. However, the calculations on the wind farm scale are based on the "instantaneous" upstream distance, updated every second with the upstream

wind direction. Similarly, the wake advection velocity is to be estimated at every second. In order to smooth the time dependence of the delay itself, the time delay is averaged for 10 minutes (or up to 10 minutes if the investigated period is shorter) during the recalibration on Thanet and validation on Horns Rev-I.

4.1.2 | Moving average of the time series

In order to avoid overfitting and starting to model the noise, both up and downstream effective wind speeds have been filtered using a moving window average with Savitzky-Golay convolution coefficients.[33] Since the objective is to model the flow behind the turbine dynamically to achieve the real-time effect, the window size was kept at 60 seconds to discard the measurement noise from the SCADA systems while avoiding oversmoothing the time series.

4.1.3 | Modelling of the meandering inside the wind farm

The wake velocity field is assumed to be axis symmetric and self-similar in the Larsen model. However, the wake meandering mechanism is shown to be significant in reducing the wake losses especially for unstable and neutral atmospheric stabilities.[34] Although the effects of meandering on a single wake profile are measured[35] and investigated heavily in the recent years,[32,36,37] the concept is still under discussion for multiple wake cases. The Dynamic Wake Meandering (DWM)[36] model transports the wake via large scale lateral and vertical components of the Mann turbulence box[38,39] and is validated on the smaller scale Egmond aan Zee wind farm.[40] On the other hand, the PossPOW algorithm uses only the SCADA data of the turbines, also to approximate the axial turbulence, and the calculations are performed on the rotor scale, instead of point-wise tracking of the wake. For that reason, a more pragmatic estimation of the meandering effect is applied.

Since the algorithm reads the individual wind direction signals at the turbine locations, the change in the lateral flow is partially taken into account. However, especially for dynamic calculations in large wind farms, the difference in the lateral turbulence between the upstream and downstream turbines is also important. Based on SCADA data only, the variance in the local wind direction signals can be used to represent the lateral turbulent effects. Therefore, Ainslie's correction to the centreline wake deficit,[34] where the meandering is correlated to the variability in the wind direction (Equation 3) empirically, is implemented in this study for both Thanet and Horns Rev-I offshore wind farms.

$$\hat{u}_{eff} = u_{eff}\left[1 + 7.12\left(\frac{\sigma_\theta}{2R_w}\right)^2\right]^{-\frac{1}{2}}, \tag{3}$$

where $\hat{u}_{eff}$ is the corrected deficit, σ_θ is the standard deviation in local wind directions, and R_w is the radius of the wake. Note that the fluctuations in the wind direction, σ_θ, are assumed to be constant for each 10 minutes, while the "nonmeandering" wake deficit, u_{eff}, and the wake radius, R_w, are updated every second.

4.1.4 | Parametrization and curve fitting

For quasi-dynamic modelling, the turbulent effects play an important role in power estimation. Similarly, for a model modified for down-regulated operations, proper representation of a highly varying c_T is also critical. The explicit formulation of the wake deficit and expansion in terms of both c_T and TI in the Larsen model is highly convenient for our application. As explained earlier, the main variables to adjust inside the wake model are c_1 and x_0, which are highly dependent on c_T and the turbulence intensity, TI. They are formulated as in Equation 4.

$$\begin{aligned} x_0 &= p_1 c_T^{p_2} + p_3 TI, \\ c_1 &= p_4 c_T^{p_5} + p_6 TI. \end{aligned} \tag{4}$$

For the fitting, the objective function combines Equation 2 and Equation 4. Together with those six parameters, it takes three inputs to predict the effective wind speed observed at the downstream turbine C02 in Thanet. The first input is the incoming effective wind speed, U_{in}, along the perpendicular direction, preprocessed using a moving average. The second input is c_T, which is tabulated in terms of wind speed as in Figure 2B and interpolated for changing U_{in} in the algorithm at every second. However, the definition of the third input, TI, is not as straightforward, especially at the downstream locations. Since the algorithm is based on turbine data only, the SCADA-based TI estimation methodology proposed in Göçmen and Giebel[13] is implemented in both Thanet and Horns Rev-I case studies. The approach employs 1-second rotor effective wind speed described above to estimate the atmospheric and local TI. The resulting turbine specific TI is tabulated in terms of incoming wind speed and local wind direction to be used in 1-second recalibration and validation cases presented in this study. Note that the ambient TI using the effective wind speed is shown to be consistently lower than the point-wise met mast measurements due to geometrical averaging over the rotor.[13] However, the corresponding correction is automatically embedded in the recalibration process.

The final parametrized non-linear functions are fitted to data using non-linear least squares approximation (NLSA). Note that this non-linearity results in parameters being highly sensitive to the initial guesses assigned. The concluding parameters together with the 95% confidence intervals are presented in Table 2. The corresponding residual plot to evaluate the goodness of fit further is presented in Figure 5. Both the scatter plot and the residuals show "missing data" around the rated region where the slope of the power curve is the highest. That is mainly due to the sensitivity of the effective wind speed method to that area, also observed in Figure 4 in Göçmen and Giebel[13] when compared with the turbines'

TABLE 2 List of model parameters and goodness of fit for the recalibration of the Larsen model: $\mathbb{R}_c^2$ is the coefficient of determination and RMSE is the root mean square error of the model predictions

p_1	**0.232 (**−57.3247, **57.7163)**
p_2	74.985 (−147.796, 148.551)
p_3	0.12 (−72.968, 78.098)
p_4	0.763 (−18.052, 41.865)
p_5	17.126 (3.182, 32.874)
p_6	4.459 (4.135, 5.255)
$\mathbb{R}_c^2 = 0.914$	RMSE = 0.718m/s

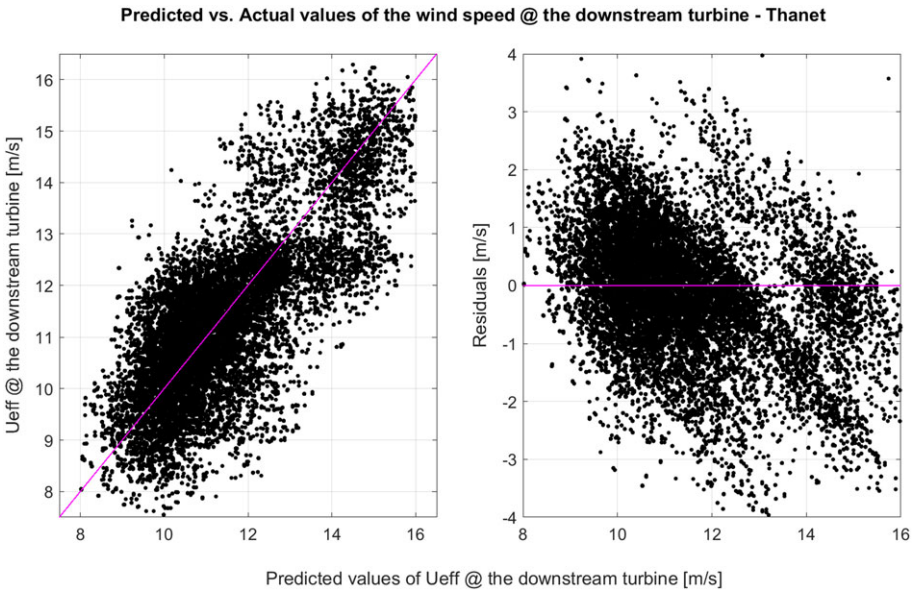

FIGURE 5 Comparison of the effective wind speed data, U_{eff}, and the recalibrated model output at the downstream turbine, distance 5.3D using 1-second training data extracted from the Thanet offshore wind farm [Colour figure can be viewed at wileyonlinelibrary.com]

original $C_P(\theta, \lambda)$ surface. Outside of that region, the model output and the 1-second training data are symmetrically distributed, both in terms of residuals and linear comparison, with a clear tendency to cluster towards the midsection of the plots.

4.1.5 | Evaluation of the fitted parameters

As stated earlier, the original Larsen model is calibrated using 10-minute averages of the flow characteristics.[18] In the previous section, the final equations are reformulated, and the parameters are fitted using 1-Hz SCADA data to simulate the observed quasi-dynamic wake effects. As a result of the considered time scales, the expansion of the wake and the velocity deficit at the downstream locations are expected to differ. A comparison of the 10-minute average and quasi-instantaneous wake shape and velocity gradient of a single wake using high fidelity actuator line large eddy simulations (LES) is presented in Machefaux et al.[41] It is seen that especially further downstream, the velocity deficit is smaller, the width of the wake is significantly larger, and the meandering effects are prominent.

The effect of the reparametrization to the wake expansion and wind speed deficits estimated by the Larsen model is presented in Figure 6. In line with the LES results, the recalibrated parameters give a broader wake behind the turbine. This is due to the widespread, high-frequency data used in the fitting that restricts the smoothing effects of conventional 10-minute averaging. Additionally, the wake deficit behind a turbine is significantly smaller as a result of meandering and consideration of the incoming wind direction at every second, instead of 10-minute averages. This tendency is observed also in the wake depth in Figure 7.

In addition to the quasi-dynamic effects to the wake shape, Figure 6 also shows a different trend with respect to higher wind speeds after recalibration. As opposed to the original Larsen model, the wake radius is decreasing with increasing wind speed, also at the above rated region, as observed in several single wake measurements (eg, Käsler et al[42] and Aitken et al[43]).

For validation, the recalibrated Larsen model is implemented in the Horns Rev-I single wake case for the easterly winds. The comparison of the original Larsen model and the recalibrated version for 1-Hz data set is presented in Figure 7. The considered period seems to have more south-easterly flow than from the north-east; therefore, the observed wake depth is not symmetrical. Note that for both versions of the model,

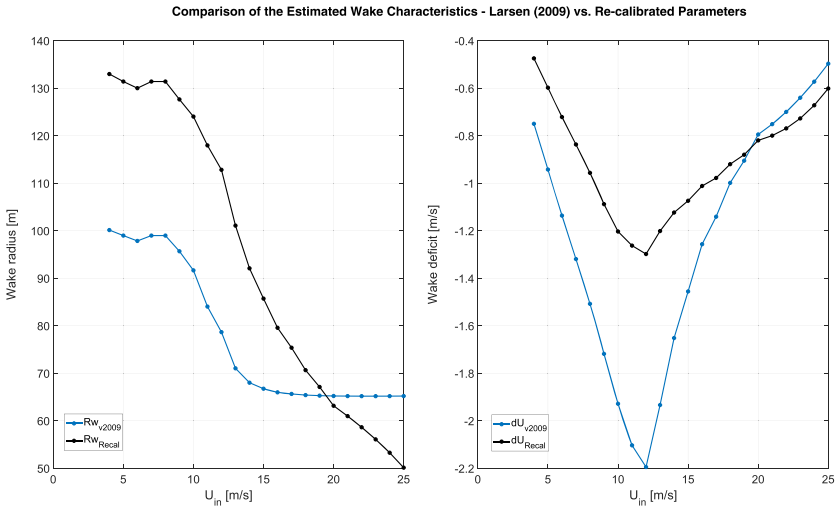

FIGURE 6 Wake expansion and the velocity deficit at 7D downstream before and after the reparametrization for real-time wake modelling, using Vestas V80-2MW power curve where Uin is the representative incoming wind speed, ambient $TI = 7\%$ [Colour figure can be viewed at wileyonlinelibrary.com]

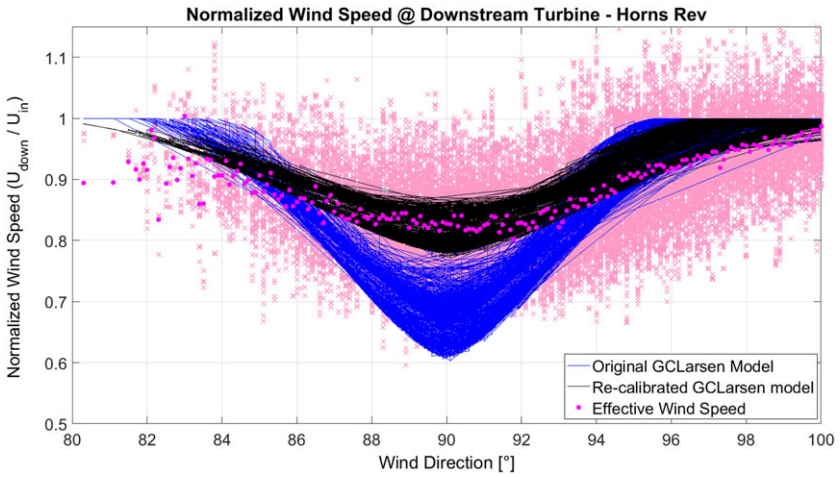

FIGURE 7 Normalized 1-second wind speed at the downstream turbine, U_{down}, distance 7D, in Horns Rev-I-original and recalibrated Larsen model together with the raw data and its moving average [Colour figure can be viewed at wileyonlinelibrary.com]

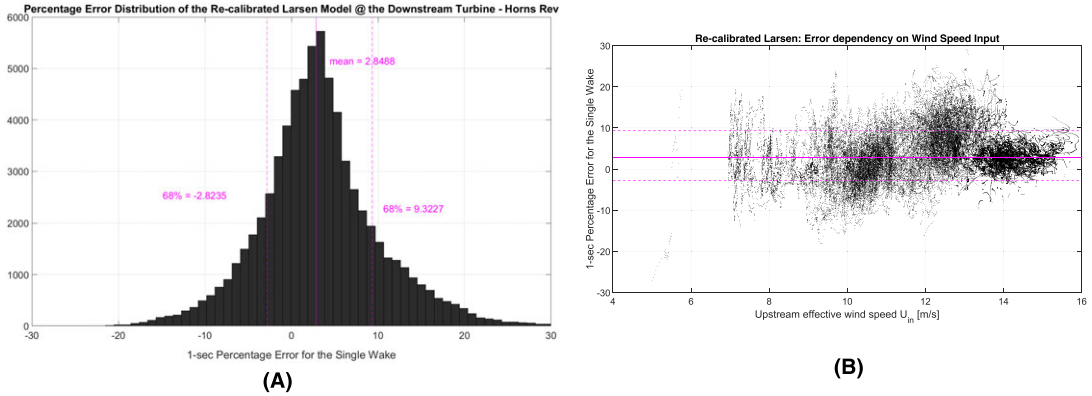

FIGURE 8 One-second percentage error distribution of the recalibrated Larsen model wind speed at the downstream turbine, distance 7D, in Horns Rev-I-$\%error_U = \frac{U_{ReLarsen} - U_{eff}}{U_{eff}} \cdot 100$. A, Distribution of 1-second percentage error: mean = 2.85% (solid line); 68% confidence intervals around the mean, −2.85% and 9.32%, respectively (dashed lines). B, Error sensitivity to the upstream effective wind speed input: mean error (solid line), 68% confidence intervals around the mean (dashed lines) [Colour figure can be viewed at wileyonlinelibrary.com]

the inputs, ie, U_{in}, c_T, and TI are the same, but the parameters c_1 and x_0 are expressed differently. Although the data is not symmetrically distributed over the wind direction span, it can easily be seen that the original Larsen model significantly underpredicts the downstream wind speed for the 1-second resolution data set. Better recovery achieved by the recalibration is observed especially for the $90^\circ \pm 5^\circ$ wind direction bin. The corresponding percentage error distribution is presented in Figure 8 where the mean 1-second error is lower than 3% with a 95% confidence bound of 15.6%. It can easily be noted that the distribution is heavily assembled around the mean error with an uncertainty of approximately 6%, where the uncertainty is defined as the half-width of the 68% confidence interval of the mean error.

The 1-second error distribution of the recalibrated wake model has a Gaussian shape with fairly broad tails, as presented in Figure 8A. The wider distribution is mainly due to the uncertainty in the wind direction that propagates during the meandering and partial wake corrections. Another source of uncertainty is the rotor effective wind speed estimation, which includes the approximation of the $C_P(\lambda, \theta)$ and the "noisy" or widespread behaviour of the 1-second SCADA data, as also seen in Figure 7 and 8B. Figure 8B also shows that positive end of the tail in the error distribution occurs around the rated region where the $C_P(\lambda, \theta)$ estimation is the most uncertain. However, it should be noted that the quantification and propagation of uncertainty in the PossPOW algorithm and the consideration of the uncertainty in the recalibration process is not included in this study in order to keep the description of the algorithm concise. Uncertainty assessment of a SCADA-based wind farm power estimation is a complex process and requires a comprehensive analysis. If interested, a further reading is encouraged (eg, Murcia Leon et al[44]).

5 | WIND FARM SCALE AVAILABLE POWER ESTIMATION

The recalibrated Larsen model is implemented to the wind farm scale where multiple and partial wakes are highly significant in evaluating the available power of the farm. The partial wake effects are considered via a weighted average over the rotor considering the rotor area influenced by the wake. For the multiple wake cases, due to the dependency of c_T to the wind speed (see Figures 2B and 3B), two different simplified approaches are applied to superpose the wakes. For the incoming wind speed below rated, since the c_T is high, only the maximum wake deficit is taken into account among contributions from all the upstream turbines at every second. Along the rated region, c_T is much lower, so all the dual deficits are aggregated via linear summation, as also suggested in Larsen et al.[45]

The time delay and the TI inside the wind farm is estimated following the same procedure as the single wake case using the raw 1-Hz turbine data without the moving average. However, while implementing the model to the wind farm scale, the effect from wake meandering is to be taken into account as described in section 4.1.3.

5.1 | Percentage error in wind speed

The percentage error in wind speed, $\%error_U = \frac{U_{ReLarsen} - U_{eff}}{U_{eff}} \cdot 100$, is estimated using the recalibrated version of the Larsen model, $U_{ReLarsen}$, which includes the corrections for the time delay and meandering and the effective wind speed calculated using the turbine operational data, U_{eff}.

Using the normal operation data set from Thanet, the averaged percentage error over different time intervals is shown in Figure 9. The arrows represent the nacelle direction signals, averaged along the same period. Note that the calculations are performed at the turbine locations only

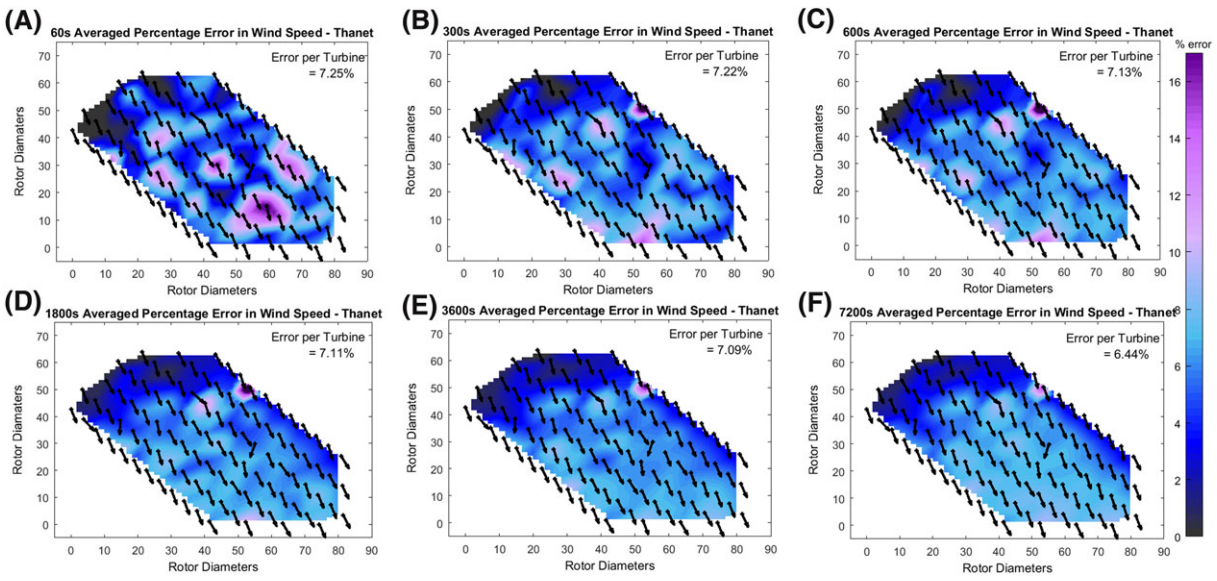

FIGURE 9 Percentage error in wind speed averaged over A, 60 seconds; B, 300 seconds; C, 600 seconds; D, 1800 seconds; E, 3600 seconds; and F, 7200 seconds across Thanet offshore wind farm. Error per turbine values correspond to the average of all the time intervals among the total period of 7 hours (ie, all 60-second intervals in 7 hours, 420 data points in total, etc) [Colour figure can be viewed at wileyonlinelibrary.com]

and linearly interpolated between the turbines to obtain a continuous error profile inside the wind farm. As expected, the model prediction error is accumulated going further downstream especially for 10-minute or longer averaging time scales. The error distribution remains nearly the same for 10-minute and larger bins with a slight flattening. The maximum prediction error is less than 16% and for most of the turbines less than 8% inside the farm. To illustrate the model error at the individual turbine level, the mean error of every single period (i, 60, 300, 600, 1800, 3600, and 7200 seconds; colour maps in Figure 9) are averaged among the whole data set of 7 hours (indicated in upper right corners in Figure 9). The averaging period of interest for the error calculations is 5 minutes in this study, following the requirements set by Danish TSO Energinet.dk.[1]

5.2 | Real-time wind speed to power

While a good agreement is achieved for the single wake and the wind farm wind speed calculations using the recalibrated Larsen wake model and the meandering correction of Ainslie, the conversion of the wind speed to power production is not straightforward. The manufacturer power curve in Figures 2B and 3B are built using 10-minute averaged power[46] (for higher resolution power curves, see Gottschall and Peinke[47]) and point-wise wind speed measurements. They are also standardized for fixed turbulence level (typically $TI = 10\%$) and air density.[46] Therefore, the approximated C_P curve using the operational pitch and rotational speed signals together with the calculated $U_{ReLarsen}$ wind speed is implemented to estimate the power production, first at the turbine and then at the wind farm level. The original $C_P(\lambda, \theta)$ surfaces for the Vestas turbines investigated were not available for this study. When provided, their implementation is strongly advised for further application of the PossPOW algorithm.

Figures 10A and 11A illustrate the comparison of the 5-minute averaged model results and the aggregated active power turbine data together with its 5% error band, as required by the Danish TSO regulations. The nominal operational data set for the Thanet case covers a period of 12 hours where for the Horns Rev-I analysis 24-hour period is presented. Especially for Thanet, the sensitivity of the PossPOW results to the inflow characteristics (ie, wind speed and direction) is clearly observed. Similar to any other wake models in the literature, the Larsen algorithm is highly affected by the wind direction uncertainty, as also reported by Gaumond et al.[48] It is clearly observed from Figure 10D that the Turbine E02 has an erroneous wind direction signal and in terms of the wake modelling perspective, the error is propagated through the model especially when it is the upstream wind direction signal. Figure 2A illustrates the layout of Thanet wind farm where the location of turbine E02 is clearly indicated. In the beginning of the 12-hour data set from Thanet, ie, for northerly winds, turbine E02 is an upstream turbine and its erroneous signal seems to induce up to a 20% modelling error during that period. Usually, the bias in the upstream wind direction signals can be corrected by adjusting the maximum wake deficit at the first downstream turbine to the perpendicular wind direction. However, for turbine E02, such a correction was unfeasible due to the lack of data to follow the centre of the wake depth at the downstream turbine. The "hit rate" refers to the ratio of points inside and outside of the ±5% error span required by the Danish grid code. Later in the investigated period, the wind becomes perpendicular to the long rows with closely spaced turbines (around 320°), which leads to stronger wakes. This can be perceived clearly by the spread in Figure 10C around time = 10 hours. Towards the end of the investigated period, the wind speed reaches the rated region where both the C_T and the approximated C_P curves are the most sensitive to the incoming wind speed.

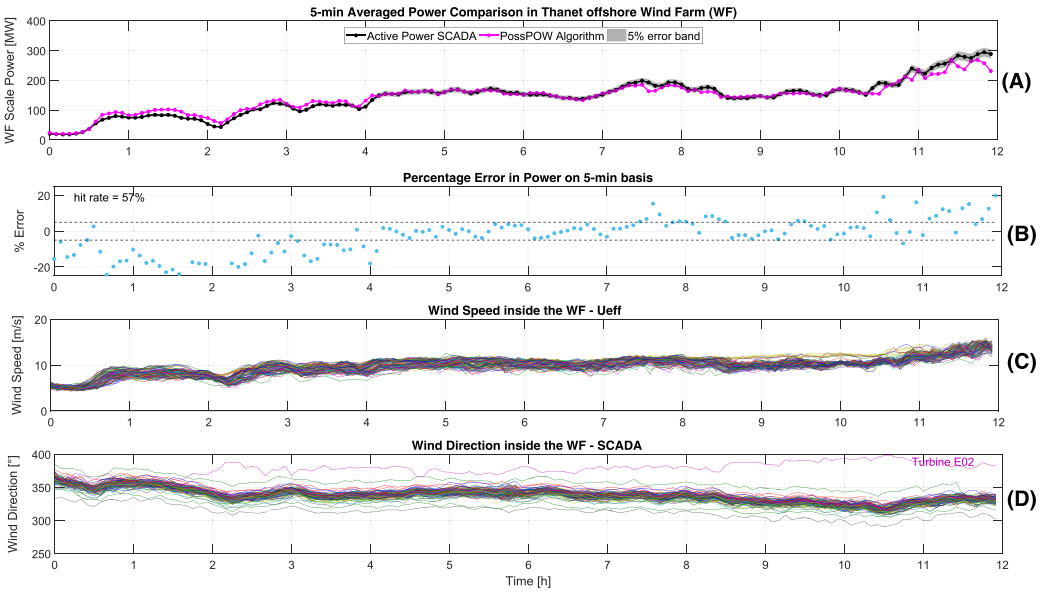

FIGURE 10 A, Five-minute averaged active power (from supervisory control and data acquisition [SCADA]) and PossPOW algorithm (re-calibrated Larsen model with generic Cp approximation) results in Thanet; B, the percentage error in 5-minute averaged power, in comparison with the Energinet.dk regulations; C, the estimated effective wind speeds at all the turbines in the wind farm; and D, the nacelle direction signals at all the turbines in Thanet, 12-hour data [Colour figure can be viewed at wileyonlinelibrary.com]

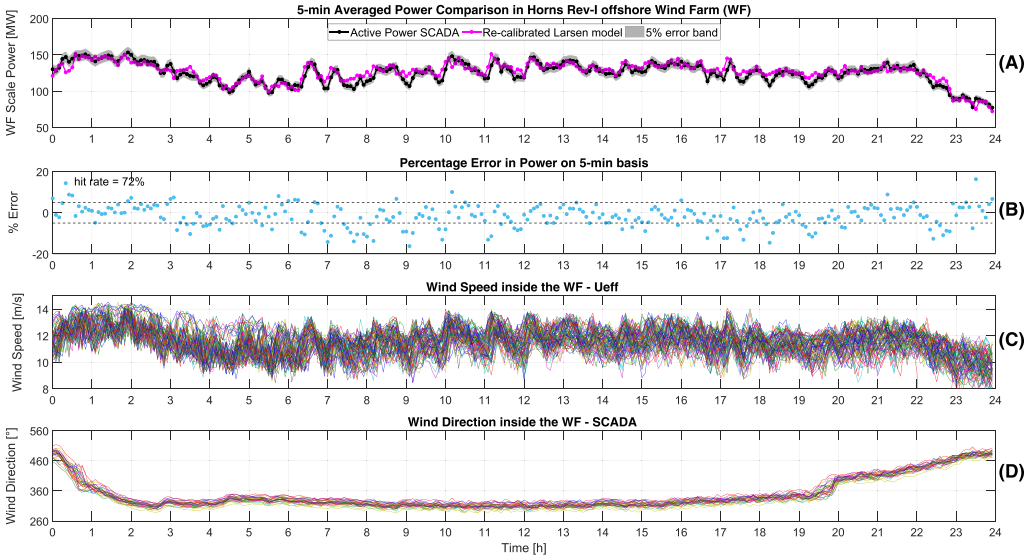

FIGURE 11 A, Five-minute averaged active power (from supervisory control and data acquisition [SCADA]) and PossPOW algorithm (re-calibrated Larsen model with generic Cp approximation) results in Horns Rev-I; B, the percentage error in 5-minute averaged power, in comparison with the Energinet.dk regulations; C, the estimated effective wind speeds at all the turbines in the wind farm; and D, the wind direction signals at all the turbines in Horns Rev-I, 24-hour data. Wind direction is augmented around 360° due to northerly winds [Colour figure can be viewed at wileyonlinelibrary.com]

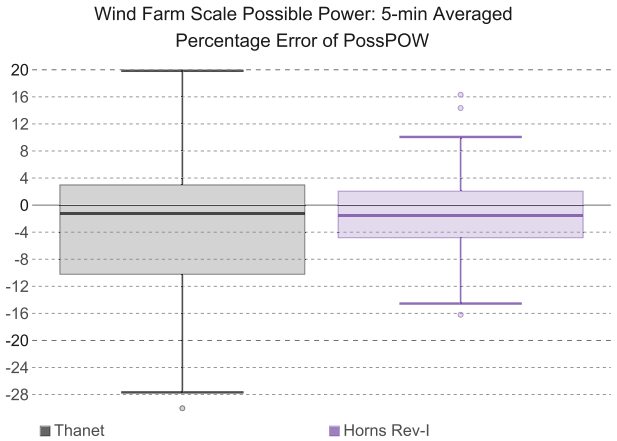

FIGURE 12 PossPOW error distribution: 12-hour data, 144 samples for Thanet and 24-hour data, 288 samples for Horns Rev-I [Colour figure can be viewed at wileyonlinelibrary.com]

The turbines in the Horns Rev-I case are exposed to north-westerly winds during the investigated period in Figure 11, which corresponds to diagonal wakes with higher turbine to turbine distances. The wind speed is slightly lower than rated with a fairly steady wind direction during the most of the data set. Given the sensitivity of the PossPOW algorithm to the wind direction and close turbine spacing observed in Thanet case, a higher hit rate and a better performance is anticipated in Horns Rev-I for the investigated period. It is also seen in Figure 11C that even for the 5-minute averaged data set, the bandwidth of the wind speed inside the wind farm is as broad as 4 m/s. This automatically corresponds to significant production differences towards downstream, indicating the importance of fast, robust, and as accurate as possible wake modelling once again. Despite the highly variable wind speed inside the wind farm, the PossPOW algorithm is seen to be in a good agreement with the data set in terms of the 5-minute averaged produced and predicted power on the wind farm scale. The strict TSO requirements regarding the quality of the wind farm scale possible power signal is met 72% of the time within 24 hour for Horns Rev-I wind farm.

The 5-minute averaged percentage error distributions for both Thanet and Horns Rev-I wind farms are presented in box plots where the boxes go from the first quartile (-0.6745σ from the mean, where σ is the standard deviation of the distribution) to the third (0.6745σ from the mean), and the middle line is the median. Representation of the median instead of the mean is simply a better measure of the error, given that the distributions are not necessarily Gaussian. The whiskers in the box plots follow Tukey's descriptive statistics[49] where the boundaries are the lowest and the highest datum within the 1.5 interquartile range (IQR) corresponding to $\pm 2.7\sigma$ from the mean. It is seen from Figure 12 that the 5-minute averaged error distribution of PossPOW for both Thanet and Horns Rev-I wind farms is assembled around zero. However, the standard deviation, which can be seen as the uncertainty of the PossPOW algorithm, is 10.5% for Thanet and 5.3% for Horns Rev-I 5-minute averaged evaluation.

6 | CONCLUSIONS

Due to the change in wake characteristics during curtailment, an estimation of the possible power of a wind farm under down-regulation is a complex process, especially for high-resolution data. Here, we present a method for real-time estimation of the wind farm possible power that draws upon the pitch and the rotational speed data together with the wind direction at the turbine location(s), valid for all operational conditions. When implemented during nominal operation, the algorithm provides a real-time (1-second resolution) wind farm power curve, which can be used in operation monitoring and wind farm controller design. In this study, the algorithm is applied and evaluated in the Thanet and Horns Rev-I offshore wind farms under nominal operation. For a down-regulated wind farm, the assessment of the possible power is highly challenging since there it is not directly measurable. However, we can benefit from the similarity in power production between the neighbouring rows in a simple layout like the Horns Rev-I wind farm. Together with the comprehensive uncertainty assessment, the experimental study to quantify the wind farm scale possible power and implementation of the PossPOW algorithm for a down-regulated wind farm is left as future work.

The available computationally affordable and robust wake models that are fast enough to be able to estimate real-time power production are designed to acquire long term, statistical information and are tuned for 10-minute averaged data. Therefore, in order to model the wind speed through the wind farm for higher time resolutions, the Larsen wake model is recalibrated. At every second, the rotor effective wind speed at the upstream and downstream turbine locations are estimated and used for both the recalibration and validation cases in Thanet and Horns Rev-I wind farms.

The recalibrated real-time wake model is implemented in the wind farm scale considering only the maximum dual wake deficit for the wind speeds lower than the rated whereas for the wind speeds above, all the wake contributions are linearly aggregated. In order to include the unsteady meandering effects especially for large offshore wind farms, the correlation of the wake deficit and the local wind direction variation introduced by Ainslie is considered. The wake loss calculations are iterated for all the turbines in the wind farm at each second and compared with the data, postprocessed for localized time delay. The percentage error in wind speed is calculated for different time averaging bins in Thanet and for shorter intervals, it is observed to be less than 8% for most of the turbines where the maximum is around 16%.

In regards to the Danish TSO requirements for compensation during periods of mandatory down-regulation, the 5-minute averaged percentage error in power was analysed when evaluating the model performance in wind farm scale power estimation. The PossPOW algorithm is shown to be in a good agreement with the active power signal, also considering the 5% error band at the power plant level as stated in the same regulation. The requirements are met for 57% of the time during 12-hour period investigated in Thanet and for 72% of the time along the 24-hour dataset in Horns Rev-I.

The PossPOW results are evaluated with respect to the wind farm and inflow characteristics as well. Overall, it is seen that the performance of the PossPOW algorithm for higher frequency possible power estimation is acceptable for below rated wind speeds on wind farms with higher turbine spacing ($\geq$7D). However, there is room for improvement for more complex flow cases around the rated and cut-in region, where the uncertainty in the SCADA data increases. Similarly, for shorter distances between upstream and downstream turbines, the fundamental far wake assumptions of the engineering wake models (ie, axisymmetric flow and "fully-developed" wake) are no longer valid. For such scenarios, the wake modelling module in the PossPOW needs to be refined. Keeping computational feasibility in mind, one of the possible advancements is to improve the recalibration process of the engineering wake models. Further recalibration enables the adaptation of wake modelling to the specific conditions of the wind turbine and/or wind farm in question with an improved accuracy. Both the implementation (eg, higher fidelity, nonoptimum performance, etc) and representation of the flow characteristics (eg, local turbulence, stability, etc) can be enhanced via further training the models using historical data. Alternatively, purely data-driven wake modelling approaches can be applied to avoid the physical limitations of the engineering models due to the simplifying assumptions. With the recent developments of machine learning algorithms, the accuracy of the PossPOW estimations can be improved with a reduced uncertainty, due to better input data handling. Together with the update of wake modelling using historical data, the quantification of the input uncertainty and its propagation through the PossPOW algorithm is considered as future work. The PossPOW algorithm already provides good estimations of the possible power as presented. It will be improved even further with the purpose of providing a more reliable available power signal in wind farm level, in terms of both the ever-tightening grid requirements and wind farm control strategies.

ACKNOWLEDGEMENTS

The authors would like to thank Pierre Elouan Réthoré (DTU Wind Energy, Roskilde, DK) and the former colleague at DTU Juan Pablo Murcia Leon (Vestas Technology, Aarhus, DK) for their valuable contributions, together with Elliot Simon (DTU Wind Energy, Roskilde, DK) for his peer review. Also Mads Rajczyk Skjelmose (Vestas Technology Aarhus, DK), Jesper Runge Kristoffersen (Vattenfall Wind Power A/S Kolding, DK), and Michael Støttrup (Siemens Gamesa Renewable Energy, Brande, DK) for provision of the 1-Hz data in both Thanet and Horns Rev-I offshore wind farms and for consultancy especially during data processing and overall revision of this work. This study is a part of the PossPOW (project no. 2012-1-10763) & Concert (project no. 2016-1-12396) projects, funded by Energinet.dk under the Public Service Obligation (PSO).

ORCID

Tuhfe Göçmen http://orcid.org/0000-0002-2510-0388

REFERENCES

1. Energinetdk. Technical regulation 3.2.5 for wind power plants with a power output above 11 kW; 2015.
2. Office of Gas and Electricity Markets, U. Grid code GC0063: power available; 2015.
3. Bundesnetzagentur. Leitfaden zum EEG-Einspeisemanagement—Abschaltrangfolge, Berechnung von Entschädigungszahlungen und Auswirkungen auf die Netzentgelte, version 2.1; 2014.
4. Göçmen T, Giebel G, Réthoré P-E, Murcia Leon J. Uncertainty quantification of the real-time reserves for offshore wind power plants. In: 15th International Workshop on Large-Scale Integration of Wind Power into Power Systems as Well as on Transmission Networks for Offshore Wind Power Plants; 2016; Vienna, Austria. http://orbit.dtu.dk/files/132541609/TuhfeGocmen_WIW2016.pdf.
5. Kristoffersen JR. The Horns Rev wind farm and the operational experience with the wind farm main controller. *Revue E-Société Royale Belge des électriciens*. 2006;122(2):26.
6. Krishna R. Available power estimator. US Patent App. 13/321 932; 2012.
7. Kazda J, Göçmen T, Giebel G, Cutululis N. Possible improvements for present wind farm models used in optimal wind farm controllers. In: 15th International Workshop on Large-Scale Integration of Wind Power into Power Systems as well as on Transmission Networks for Offshore Wind Power Plants; 2016; Vienna, Austria. http://orbit.dtu.dk/files/127985413/WIW16_0107_posterpaper_Kazda.pdf.
8. Annoni J, Gebraad PM, Scholbrock AK, Fleming PA, Wingerden JWV. Analysis of axial-induction-based wind plant control using an engineering and a high-order wind plant model. *Wind Energy*. 2016;19(6):1135-1150.
9. Goit JP, Meyers J. Optimal control of energy extraction in wind-farm boundary layers. *J Fluid Mech*. 2015;768:5-50.
10. Goit JP, Munters W, Meyers J. Optimal coordinated control of power extraction in LES of a wind farm with entrance effects. *Energies*. 2016;9(1):1-20.
11. PossPOW: Possible Power of Offshore Wind power plants. http://www.posspow.vindenergi.dtu.dk
12. Göçmen T, Giebel G, Poulsen NK, Mirzaei M. Wind speed estimation and parametrization of wake models for downregulated offshore wind farms within the scope of PossPOW project. In: Journal of Physics: Conference Series, Vol. 524; 2014; Copenhagen, Denmark. https://doi.org/10.1088/1742-6596/524/1/012156
13. Göçmen T, Giebel G. Estimation of turbulence intensity using rotor effective wind speed in Lillgrund and Horns Rev-I offshore wind farms. *Renewable Energy*. 2016;99:524-532.
14. Crespo A, Hernández J, Frandsen ST. Survey of modelling methods for wind turbine wakes and wind farms. *Wind Energy*. 1999;2(1):1-24.
15. Vermeer LJ, Sørensen JN, Crespo A. Wind turbine wake aerodynamics. *Prog Aerosp Sci*. 2003;39(6):467-510.
16. Göçmen T, Laan PVD, Réthoré PE, Diaz AP, Larsen GC, Ott S. Wind turbine wake models developed at the Technical University of Denmark: a review. https://doi.org/10.1016/j.rser.2016.01.113; 2016.
17. Larsen GC. A simple wake calculation procedure. *Risø-M*. 1988;No. 2760:58. http://orbit.dtu.dk/ws/files/55567186/ris_m_2760.pdf
18. Larsen GC. A simple stationary semi-analytical wake model. *Denmark. Forskningscenter Risoe. Risoe-R*. 2009;1713(August):1-21.
19. Bastankhah M, Porté-Agel F. A new analytical model for wind-turbine wakes. *Renewable Energy*. 2014;70:116-123.
20. Japar F, Mathew S, Narayanaswamy B, Lim CM, Hazra J. Estimating the wake losses in large wind farms: a machine learning approach. In: 2014 IEEE PES Innovative Smart Grid Technologies Conference, ISGT 2014; 2014; Washington, DC, USA:1-5. https://doi.org/10.1109/ISGT.2014.6816427
21. A/S VWS. Vestas V90 3 MW. Brochure. http://nozebra.ipapercms.dk/Vestas/Communication/Productbrochure/V9030MW/V9030MWUK/; 2017.
22. A/S VWS. Vestas V80 2 MW. Brochure. URL https://www.ledsjovind.se/tolvmanstegen/Vestas%20V90-2MW.pdf; 2011.
23. Göçmen T, Giebel G, Sørensen P, Poulsen N. Possible power estimation of down-regulated offshore wind power plants. *PhD Thesis*: Technical University of Denmark, Department of Wind Energy; 2016.
24. Hansen KS, Barthelmie RJ, Jensen LE, Sommer A. The impact of turbulence intensity and atmospheric stability on power deficits due to wind turbine wakes at Horns Rev wind farm. *Wind Energy*. 2012;15(1):183-196.
25. Nygaard NG. Wakes in very large wind farms and the effect of neighbouring wind farms. In: Journal of Physics: Conference Series, Vol. 524; 2014; Copenhagen, Denmark. https://doi.org/10.1088/1742-6596/524/1/012162
26. Zahle F, Sørensen NN. Characterization of the unsteady flow in the nacelle region of a modern wind turbine. *Wind Energy*. 2011;14(2):271-283.
27. Beltrán J, Guerrero JJ, Melero JJ, Llombart A. Detection of nacelle anemometer faults in a wind farm minimizing the uncertainty. *Wind Energy*. 2013;16(6):939-952.
28. Barthelmie RJ, Larsen GC, Frandsen ST, et al. Comparison of wake model simulations with offshore wind turbine wake profiles measured by Sodar. *J Atmos Oceanic Technol*. 2006;23(7):888-901.
29. Sanderse B, van der Pijl SP, Koren B. Review of computational fluid dynamics for wind turbine wake aerodynamics. *Wind Energy*. 2011;14(7):799-819.
30. Christiansen MB, Hasager CB. Wake effects of large offshore wind farms identified from satellite SAR. *Remote Sens Environ*. 2005;98(2-3):251-268.
31. Gaumond M, Réthoré PE, Bechmann A, et al. Benchmarking of wind turbine wake models in large offshore wind farms. { … } Torque from Wind { … }, http://www.eera-dtoc.eu/wp-content/uploads/files/Gaumond-et-al-Benchmarking-of-wind-turbine-wake-models-in-large-offshore-wind-farms5.pdf; 2012.
32. Machefaux E, Larsen GC, Troldborg N, Gaunaa M, Rettenmeier A. Empirical modeling of single-wake advection and expansion using full-scale pulsed lidar-based measurements. *Wind Energy*. 2015;18(12):2085-2103.
33. Savitzky A, Golay MJE. Smoothing and differentiation of data by simplified least squares procedures. *Anal Chem*. 1964;36(8):1627-1639.
34. Ainslie JF. Wake modelling and the prediction of turbulence properties. In: Proceedings of the BWEA Wind Energy Conference (British Wind Energy Association); 1986:115-120.
35. Bingöl F., Mann J, Larsen GC. Light detection and ranging measurements of wake dynamics Part I: one-dimensional scanning. *Wind Energy*. 2010;13(1):51-61.
36. Larsen GC, Madsen HA, Thomsen K, Larsen TJ. Wake meandering: a pragmatic approach. *Wind Energy*. 2008;11(4):377-395.

37. Madsen HA, Larsen GC, Larsen TJ, Troldborg N, Mikkelsen R. Calibration and validation of the dynamic wake meandering model for implementation in an aeroelastic code. *J Solar Energy Eng*. 2010;132(4):041014.
38. Mann J. The spatial structure of neutral atmospheric surface-layer turbulence. *J Fluid Mech*. 1994;273:141-168.
39. Mann J. Wind field simulation. *Probab Eng Mech*. 1998;13(4):269-282.
40. Larsen TJ, Madsen HA, Larsen GC, Hansen KS. Validation of the dynamic wake meander model for loads and power production in the Egmond aan Zee wind farm. *Wind Energy*. 2013;16(4):605-624.
41. Machefaux E, Larsen GC, Troldborg N, Rettenmeier A. Single wake meandering, advection and expansion—an analysis using an adapted pulsed lidar and CFD LES-ACL simulations. In: European Wind Energy Conference and Exhibition, EWEC 2013, Vol. 2; 2013:1016-1026. URL http://www.scopus.com/inward/record.url?eid=2-s2.0-84903479783&partnerID=tZOtx3y1
42. Käsler Y, Rahm S, Simmet R, Kühn M. Wake measurements of a multi-MW wind turbine with coherent long-range pulsed Doppler wind lidar. *J Atmos Oceanic Technol*. 2010;27(9):1529-1532.
43. Aitken ML, Banta RM, Pichugina YL, Lundquist JK. Quantifying wind turbine wake characteristics from scanning remote sensor data. *J Atmos Oceanic Technol*. 2014;31(4):765-787.
44. Murcia Leon J, Réthoré PE, Natarajan A, Sørensen J. Uncertainty quantification in wind farm flow models. *PhD Thesis*. Denmark: Technical University of Denmark, Department of Wind Energy; 2017.
45. Larsen TJ, Larsen GC, Aagaard Madsen H, Petersen SM. Wake effects above rated wind speed. An overlooked contributor to high loads in wind farms. In: Scientific Proceedings, EWEA Annual Conference and Exhibition; 2015; Paris, France:95-99.
46. IEC. IEC international standard, IEC 61400-12-1, wind turbines—part 12-1 : power performance measurements of electricity producing wind turbines. *Int Electrotech Commission*. 2005;2005:179.
47. Gottschall J, Peinke J. How to improve the estimation of power curves for wind turbines. *Environ Res Lett*. 2008;3(1). http://iopscience.iop.org/article/10.1088/1748-9326/3/1/015005/meta.
48. Gaumond M, Réthoré PE, Ott S, Peña A, Bechmann A, Hansen KS. Evaluation of the wind direction uncertainty and its impact on wake modeling at the Horns Rev offshore wind farm. *Wind Energy*. 2014;17(8):1169-1178.
49. Tukey JW. The future of data analysis. *Ann Math Stat*. 1962;33(1):1-67.

How to cite this article: Göçmen T, Giebel G, Poulsen NK, Sørensen PE. Possible power of down-regulated offshore wind power plants: The PossPOW algorithm. *Wind Energy*. 2019;22:205–218. https://doi.org/10.1002/we.2279